Soft Matter

Cite this: DOI: 10.1039/c0sm01079k

www.rsc.org/softmatter

PAPER

Discovering multicore micelles: insights into the self-assembly of linear *ABC* terpolymers in midblock-selective solvents

Liquan Wang and Jiaping Lin*

Received 29th September 2010, Accepted 15th December 2010
DOI: 10.1039/c0sm01079k

Using self-consistent field calculations, multicore micelles, such as the double-stranded superhelix, were discovered from the solution-state self-assembly of linear *ABC* terpolymers consisting of a solvophilic midblock and two mutually incompatible solvophobic endblocks. The multicore micelles were formed when the *A* and *C* endblocks self-associated into multiple incompatible solvophobic cores that were subdivided alternately by solvophilic *B* domains, thereby constructing hierarchical packing. The structures emerged depended on the relative lengths of the blocks and the solubility of the midblocks. According to the calculation results, diagrams of the observed structures as a function of the block length and midblock solubility were constructed. The results obtained can enrich our existing knowledge of the hierarchical assembly of copolymers and provide useful information for mimicking complex biological systems.

I. Introduction

Hierarchical assembly, which allows molecular packing and structural ordering at multiple length scales, has recently drawn great research interest.[1–5] Inspired by complex biological systems, such as those of proteins, the concept of multicompartment micelles with hierarchical microstructures has emerged beyond the conventional micelle-like aggregates with morphologies ranging from spheres to cylinders, and vesicles, *etc*.[6–9] Amphiphilic *ABC* terpolymers containing three mutually immiscible blocks have been identified to serve as straightforward model systems for building multicompartment micelles. For instance, *ABC* miktoarm star terpolymers[10–15] and linear terpolymers[16–21] have been reported to be capable of forming multicompartment micelles, such as hamburger micelles and segmented wormlike micelles in selective solvents. The exhibited microstructures were composed of a solvophilic shell and a phase-separated solvophobic core with common interfaces between distinct solvophobic domains, as schematically shown in Fig. 1a. Recent studies have shown other intricate compartmentalized micelles whose solvophobic cores are segregated by solvophilic domains (Fig. 1b), such as cylindrical nanostructures with alternating solvophilic–solvophobic layers[22] and the double-stranded superhelix.[23] These micelles are formed from the complexation of charged solvophilic blocks with multiamine counterions, and their inner structures are shown to miss the common interface between different solvophobic domains but still remain regularly organized. Thus, a concept of multicore micelles is proposed so as to differ from the multicompartment micelles. Systems with such a core-packing motif are of great interest both in theory and in application, particularly in mimicking complex biological systems, such as proteins.

A linear *ABC* terpolymer combining a solvophilic midblock and two mutually incompatible solvophobic endblocks is a promising molecular model for multicore micelles in selective solvents. As sketched in Fig. 1c, due to the fact that both ends are fixed to two mutually incompatible solvophobic blocks, the solvophilic midblock cannot spread freely into the surrounding solvent media. Rather, it must simultaneously bridge the different solvophobic domains and screen the solvophobic cores from the solvent environment, thereby constructing a regular multicore micelle with alternating solvophilic–solvophobic structures. However, so far, little attention has been paid to *ABC* terpolymers with such solvophobic–solvophilic–solvophobic (*HPH*) sequences.[24–28] In the experimental aspect, Laschewsky *et al.* recently reported an observation of a raspberry-like micelle with multicore characteristics by cryogenic transmission electron microscopy.[25,26] The raspberry-like micelles are self-assembled from the *ABC* terpolymers with *HPH* sequence. Despite this study, a systematical experimental study of the multicore micelles from the self-assembly of *HPH ABC* terpolymer solutions still presents several challenges. First, the careful morphological visualization of complex micelles, especially distinguishing the multicore micelles from the multicompartment micelles, presents a challenge in experiments.[10,29] Second, a systematical study needs the tuning of a large number of parameters such as copolymer compositions and monomer–monomer interactions. This requires the synthesis of a series of terpolymers. Therefore, a systematically experimental exploration of the self-assembly

Shanghai Key Laboratory of Advanced Polymeric Materials, State Key Laboratory of Bioreactor Engineering, School of Materials Science and Engineering, East China University of Science and Technology, Shanghai, 200237, China. E-mail: jplinlab@online.sh.cn; jlin@ecust.edu.cn; Fax: +86-21-64251644; Tel: +86-21-64253370

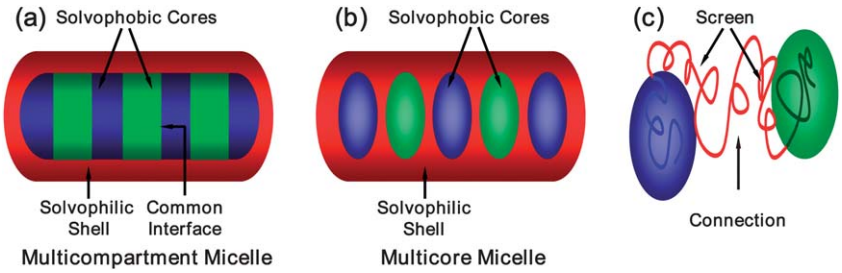

Fig. 1 Schematic of (a) a multicompartment micelle and (b) a multicore micelle. The blue and green regions denote solvophobic cores and the red region denotes a solvophilic shell. (c) Sketch of the effect of a solvophilic midblock of a linear *ABC* terpolymer. The solvophilic midblock (red) simultaneously screens and connects the individual solvophobic cores (blue and green).

behaviors of *HPH ABC* terpolymer solutions is a rather challenging task. In contrast with experiments, theory and simulation provide an ideal tool for identifying the detailed microscopic structures and exploring the phase space of *HPH ABC* terpolymer solutions. In particular, theory and simulation can provide a good understanding of the underlying principles governing this self-assembly on a molecular level. These principles are of fundamental importance to controlling the formation of hierarchical multicore micelles and guiding the future experiments.

The self-consistent field (SCF) theory has been proven to be a powerful tool to characterize the equilibrium thermodynamic features of copolymers with diverse architectures[30–38] as well as mixtures of copolymers with additives such as homopolymers,[39] copolymers,[40] and nanoparticles.[41–43] Moreover, the SCF theory is capable of capturing the essential characteristic of the self-assembly of copolymers in dilute solutions.[44–49] With the assistance of the real-space method proposed by Fredrickson *et al.*,[31] Liang and coworkers investigated the aggregation behavior of amphiphilic diblock copolymers in selective solvents.[45,46] Vesicles and micelles were observed by tailoring the parameters such as the polymer composition, initial density fluctuation, and polydispersity. In addition, this SCF method was also used to study solution-state self-assembly of more complicated copolymers such as triblock copolymers.[18] In our previous work, we have utilized the real-space SCF theory to study the self-assembly behaviors of amphiphilic graft copolymers and block copolymer/nanoparticle mixtures in dilute solutions.[47,48] The simulation results are found to be in good agreement with the experimental observations. However, so far, most of the SCF works reported have been performed in two dimensions, and therefore the information provided could be limited. Specifically, for identifying the complex structures of multicore micelles, a three-dimensional calculation is needed.

In this work, a three-dimensional real-space SCF theory was employed to investigate the multicore micelles formed by linear *ABC* copolymers in a midblock-selective solvent. Various multicore micelles such as the superhelix were found. Influences of the length of blocks and the solubility of midblocks on the morphologies of multicore micelles were studied. Based on the calculation results, the observed aggregate structure regions as a function of the block length and midblock solubility were also constructed. A free energy analysis was carried out toward the novel superhelical structures. The superhelix was found to be stable at intermediate solubility of the midblocks, arising from the interplay of enthalpic and entropic effects. Finally, the SCF results were compared with the available experimental results. The SCF theory can not only reproduce the experimental results, but also provide a deep insight into the experimental phenomena.

II. Theoretical methods

We consider a system (with volume, V) of amphiphilic linear *ABC* terpolymers dissolved in solvents, S. Each copolymer consists of a *B* solvophilic midblock and two mutually incompatible solvophobic *A* and *C* endblocks. The relative lengths of the *A*, *B*, and *C* blocks are f_A, f_B, and f_C, respectively. The terpolymers are assumed to be monodisperse with the total degree of polymerization N. The solvent, S, is a short homopolymer chain possessing σN monomers, where the σ is the ratio of the solvent size to polymer size.[49] The volume fraction of linear *ABC* terpolymer is c_P, and thus the volume fraction of solvent is $1 - c_P$.

In the SCF theory, the configuration of a single terpolymer chain and solvent is determined by a set of effective chemical potential fields, $\omega_i(r)$, where the suffix, i, stands for block species *A*, *B*, *C*, and S. An incompressibility modulus, $\xi(\mathbf{r})$, is invoked to ensure that the local density $\left(\sum_{i=A,B,C,S}\varphi_i(\mathbf{r})\right)$ is a constant. The free energy density (in units of k_BT) of the system is described as follows:

$$F = -c_P \ln\left(\frac{Q_P}{V}\right) - N(1-c_P)\ln\left(\frac{Q_S}{V}\right) + \frac{1}{V}\int d\mathbf{r}\left[\frac{1}{2}\sum_{\substack{i,j=A,B,C,S \\ i\neq j}}\chi_{ij}N\varphi_i(\mathbf{r})\varphi_j(\mathbf{r}) - \sum_{i=A,B,C,S}\omega_i(\mathbf{r})\varphi_i(\mathbf{r}) - \xi(\mathbf{r})\left(1-\sum_{i=A,B,C,S}\varphi_i(\mathbf{r})\right)\right] \quad (1)$$

In this expression, χ_{ij} is the Flory–Huggins parameter characterizing the interactions between different species i and j. $Q_P = \int d\mathbf{r} q(\mathbf{r},1)$ is the partition function for a single chain subject to the effective chemical potential field, $\omega_i(\mathbf{r})$(i = *A*, *B*, *C*), in terms of propagators, $q(\mathbf{r},s)$. The spatial coordinate, $\mathbf{r}$, is rescaled by R_g, where $R_g^2 = a^2N/6$ (a is the statistical segment length). The contour length is parameterized with variable t, which starts from one end ($t = 0$) to the other ($t = 1$). The propagators $q(\mathbf{r},t)$and $\bar{q}(\mathbf{r},t)$ satisfy the following modified diffusion equations:

$$\frac{\partial q(\mathbf{r},t)}{\partial t} = \left[R_g^2\nabla^2 - \omega_{\theta(t)}(\mathbf{r})\right]q(\mathbf{r},t)$$
$$-\frac{\partial \bar{q}(\mathbf{r},t)}{\partial t} = \left[R_g^2\nabla^2 - \omega_{\theta(t)}(\mathbf{r})\right]\bar{q}(\mathbf{r},t) \quad (2)$$

with the initial condition $q(\mathbf{r},0) = 1$ and $\bar{q}(\mathbf{r},1) = 1$, respectively. Here, $\theta(t)$ is used to specify the segment type along the copolymer chain, subject to

$$\theta(t) = \begin{cases} A & \text{if} \quad 0 < t < f_A \\ B & \text{if} \quad f_A < t < f_A + f_B \\ C & \text{if} \quad f_A + f_B < t < 1 \end{cases} \quad (3)$$

Q_S is the partition function for a solvent in the field $\omega_S(\mathbf{r})$, which is given by

$$Q_S = \int d\mathbf{r} q_S(\mathbf{r},\sigma) \quad (4)$$

As for the terpolymer chain, the $q_S(\mathbf{r},t)$ satisfies the following modified diffusion equation:

$$\frac{\partial q_S(\mathbf{r},t)}{\partial t} = \left[R_g^2\nabla^2 - \omega_S(\mathbf{r})\right]q_S(\mathbf{r},t) \quad (5)$$

subject to initial condition $q_S(\mathbf{r},0) = 1$.

In terms of the single-chain propagators, the segment densities follow that

$$\varphi_i(\mathbf{r}) = \frac{Vc_P}{Q_P}\int_{t\in i} dt q(\mathbf{r},t)\bar{q}(\mathbf{r},t) \quad i = A,B,C \quad (6)$$

$$\varphi_S(\mathbf{r}) = \frac{V(1-c_P)}{Q_S}\int_0^\sigma dt q_S(\mathbf{r},t)q_S(\mathbf{r},\sigma-t) \quad (7)$$

Minimization of free energy F with respect to $\varphi_i(\mathbf{r})(i = A, B, C, S)$ and $\xi(\mathbf{r})$, can lead to a set of mean-field equations:

$$\omega_i(\mathbf{r}) = \sum_{\substack{j=A,B,C,S \\ j\neq i}} \chi_{ij}N\varphi_j(\mathbf{r}) + \xi(\mathbf{r}) \quad i = A,B,C,S \quad (8)$$

$$\sum_{i=A,B,C,S}\varphi_i(\mathbf{r}) = 1 \quad (9)$$

The free energy can be decomposed into

$$F = U - TS \quad (10)$$

Here, U and S are the internal energy contribution and configurational entropy contribution to free energy, respectively. These quantities are given by

$$U = \frac{1}{2}\sum_{\substack{i,j=A,B,C,S \\ i\neq j}} \frac{\chi_{ij}N}{V}\int d\mathbf{r}\varphi_i(\mathbf{r})\varphi_j(\mathbf{r}) \quad (11)$$

$$-TS = -c_P\ln\left(\frac{Q_P}{V}\right) - N(1-c_P)\ln\left(\frac{Q_S}{V}\right) - \sum_{i=A,B,C,S}\frac{1}{V}\int d\mathbf{r}\omega_i(\mathbf{r})\varphi_i(\mathbf{r}) \quad (12)$$

For the purpose of finding the self-consistent solution, a variant of the algorithm developed by Fredrickson and co-workers was adopted.[50–52] The calculation was carried out in three dimensions with periodic boundary. The spatial resolutions were taken to be smaller than $R_g/4$ and the contour was discretized with 100 steps.[44,45] The calculations started from a homogeneous state with a small initial fluctuation amplitude value on the order of 10^{-8} in three dimensions. The diffusion eqns (2) and (5) were solved with the Baker–Hausdorff operator splitting formula proposed by Rasmussen *et al.*[53,54] In addition, the potential fields, $\varphi_i(\mathbf{r})$, and pressure field $\xi(\mathbf{r})$ were updated by means of a two-step Anderson mixing scheme.[55] The simulation proceeded until the relative accuracy in the field (measured by $\sqrt{\sum_i \int d\mathbf{r}(\omega_i^{new}(\mathbf{r}) - \omega_i^{old}(\mathbf{r}))^2 / \sum_i \int d\mathbf{r}}$). reached 10^{-6} and a condition of incompressibility was achieved.[56] The simulations were repeated 10–20 times from the homogeneous solution with different initial states to ensure that the observed phenomena are not accidental.[46,57]

III. Results and discussion

In the present work, we examined the self-assembly behavior of linear *ABC* terpolymers in midblock-selective solvents. Without specification, the volume fraction of terpolymers c_P is set to be 0.10. The *A*, *B*, and *C* blocks of linear *ABC* terpolymers are mutually incompatible and the Flory–Huggins parameters are set as $\chi_{AB}N = \chi_{BC}N = \chi_{AC}N = 20.0$. In addition, the two *A* and *B* endblocks are set to be solvophobic with $\chi_{AS}N = \chi_{CS}N = 40.0$. The ratio of the solvent size to polymer size is assumed to be $\sigma = 0.05$. In the SCF calculations, the relative lengths of different blocks and the solubility of the *B* midblock are variable.

SCF calculations reveal that the linear *ABC* copolymers can self-assemble into various complex multicore micelles in midblock-selective solvents. Fig. 2 shows a typical assembly from linear *ABC* terpolymers with a relative *B* block length of 0.20 and

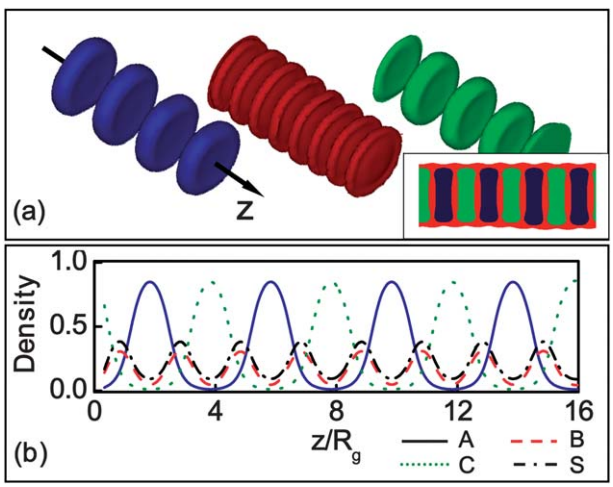

Fig. 2 (a) A super-cylinder self-assembled from linear *ABC* terpolymers in a selective solvent with $f_A = f_C = 0.40$ and $\chi_{BS}N = 2.0$. The blue, red, and green colors are assigned to *A*, *B*, and *C* blocks, respectively. The outermost surface of solvophilic *B* blocks is not shown to clearly present the inner structures. The inset shows a two-dimensional structure along the *z* axis. (b) Density profile on a cross section of the super-cylinder which is marked with an arrow shown in (a).

equal relative lengths of *A* and *C* blocks. This assembly exhibits a super-cylindrical microstructure, where the *A* and *C* blocks self-assemble into oblate disk-like cores surrounded by the *B* shell (Fig. 2a). Noteworthy, this assembly is not the widely-observed solvophobic core/solvophilic shell microstructures, but rather a cylinder consisting of alternating solvophobic and solvophilic disks packed perpendicular to the cylindrical axis, as indicated in Fig. 2b. We designated this super-cylinder as **DDC**, where **D** (disk), **D**, and **C** (cylinder) represent the structures of the *A* core, *C* core, and whole scale, respectively. The designation of other structures also follows this rule.

In addition to the **DDC**, a rich variety of multicore micelles were found when the relative lengths of the blocks were changed. The observed results were summarized into a morphology-composition diagram, which is shown in Fig. 3. The microstructures of the multicore micelles discovered are as follows: sphere with *A* and *C* helix-like cores (**HHS**), sphere with *A* and *C* disk-like cores (**DDS**), cylinder with *A* ring-like core and *C* disk-like core (**RDC**), cylinder with *A* and *C* ring-like cores (**RRC**), cylinder with *A* spherical core and *C* cylindrical core (**SCC**), sphere with *A* and *C* spherical cores (**SSS**), and special vesicle with irregular *A*-patches residing near the core/corona interface and *A*-tubes embedding within the central core region (**SV**). These structures share a common packing feature: the *A* and *C* solvophobic cores are alternately packed, while the solvophilic *B* midblocks occupy both the interspaces and the outermost surface to shield each solvophobic core from solvent media. Fig. 3 also reveals a variety of morphological transitions that the linear *ABC* terpolymer undergoes in selective solvents. For example, a morphological transition of **DDS** → **DDC** → **RRC** → **SSS** was observed with increasing f_B when $f_A = f_C$.

From Fig. 3, it can be noted that the cylindrical micelles such as **DDC** were presented to be without ends. This is because the length of cylindrical micelles far exceeded the size of the simulation box. This also means that the longer cylinders are favored in the calculations. Actually, the ends are important for cylindrical micelles, which determine the size of cylindrical micelles. To observe the ends of cylindrical micelles, we recalculated **DDC** structures in a larger simulation box. Since the size of micelles depends on the length of the midblock, we presented the results for multicore micelles at various volume fractions of midblock, as shown in Fig. 4. When the midblock is short ($f_B = 0.05$), a **DDS** structure was observed. With increasing the midblock length, the **DDS** is extended and changed into a spindle-like **DDS** structure ($f_B = 0.10$). As the midblock length continues to increase, the spindle-like structure is further extended and turned into a cylinder-shaped **DDC** micelle with ends ($f_B = 0.18$). Notably, there is no clear distinction between **DDS** and **DDC**, and the **DDS** can be considered to be the limit case of **DDC** with a short midblock. As the midblock length further increases, the cylinders with no ends were found (as can be seen in Fig. 2 and 3), since the longer size of cylinders exceeds the size of the simulation box. The information concerning the ends of longer cylinders can be obtained from the cylinders at a relatively shorter midblock.

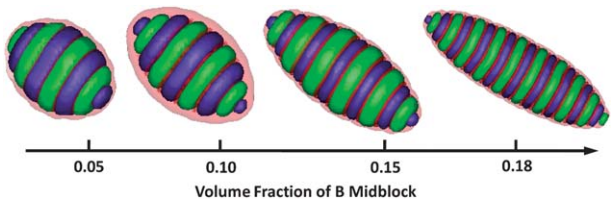

Fig. 4 Multicore micelle structures as a function of the volume fraction of *B* midblocks for linear *ABC* terpolymers with equal lengths of *A* and *C* endblocks in a selective solvent. Other parameter is $\chi_{BS}N = 2.0$. The colors appear as in Fig. 2.

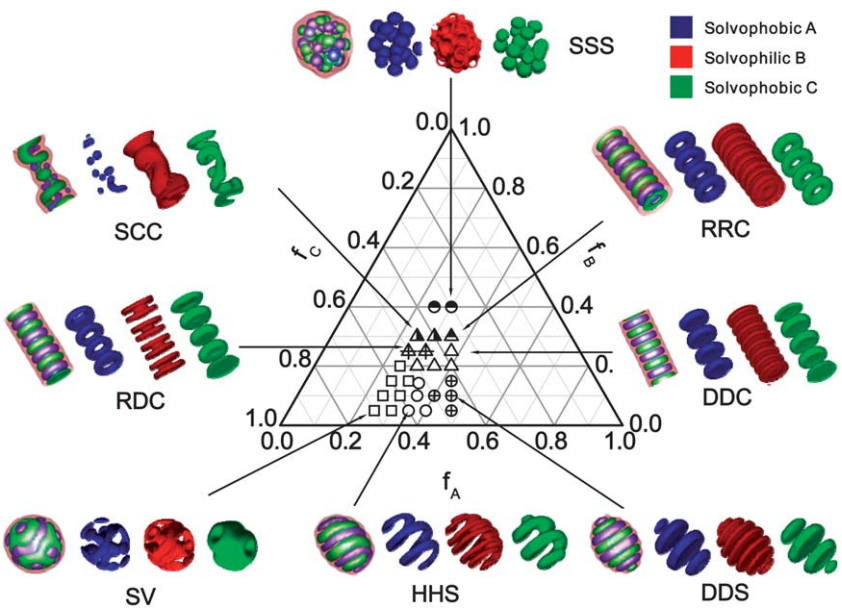

Fig. 3 Observed structure regions for linear *ABC* terpolymers in a selective solvent with $\chi_{BS}N = 2.0$. The terms f_A, f_B, and f_C are the relative lengths of the *A*, *B*, and *C* blocks, respectively. From left to right, each inset shows the structures that arise from the whole molecules, *A*, *B* (inner structure without outermost surface), and *C* blocks, respectively. **SV** is a special vesicle with irregular *A*-patches residing near the core/corona interface and *A*-tubes embedding within the central core region. In other representations, the first, second, and last letters are denoted as the structures of the *A* core, *C* core, and large length scales, respectively.

Analyzing the observed microstructures reveals that hierarchy is a distinct feature of multicore micelles. This hierarchy can be further understood by considering the microstructures at two different length scales. First, the midblocks favor the formation of isolated cores from the solvophobic A and C blocks at small-length-scale orders. The solvophilic B midblock allows the manipulation of the interfacial curvature in these small-length-scale aggregates, producing a series of local geometries. Three classical morphologies, including sphere-like substructures, cylinder-like substructures, and disk-like substructures, are observed. The local morphologies may vary across these three structures when the relative lengths of the solvophilic midblocks are changed. Second, solvophilic midblocks impose an important chain constraint on the small-length-scale cores and drive them to organize into large-length-scale orders. In the ordered large-length-scale microstructure, the midblocks are arranged more regularly than a relatively disordered microstructure, so that the optimal chain-packing motif has the minimum required stretching energy of midblocks around the solvophobic cores. The large-length-scale structures are greatly dependent on the length of the midblock. For instance, when $f_A = f_C$, with increasing the relative midblock lengths, the large-length-scale structures change from spheres into cylinders, while the small-length-scale structures remain disk-like (**DDS** → **DDC**).

The microstructure of multicore micelles can also be manipulated by the solubility of the B midblock ($\chi_{BS}N$). To illustrate the effect of $\chi_{BS}N$, we calculated the influence of changing $\chi_{BS}N$ on the formed microstructure and mapped out the aggregate morphology regions in f_B-$\chi_{BS}N$ space for linear ABC terpolymers with equal lengths of A and C blocks in selective solvents, which is shown in Fig. 5. Each point corresponds to a simulation result, and the lines are drawn to show the boundaries between different structures. The solubility of the midblock has a marked influence on the microstructures. At higher values of f_B, it was found that the microstructures can be tuned from **RRC** to superhelix to **DDC** by increasing the $\chi_{BS}N$ value. However, at lower f_B values, only the **DDC** → **DDS** transition was observed when the $\chi_{BS}N$ value increases. Overall, the boundaries between different structures show a shift to a higher value of $\chi_{BS}N$ as the relative length of the midblock increases.

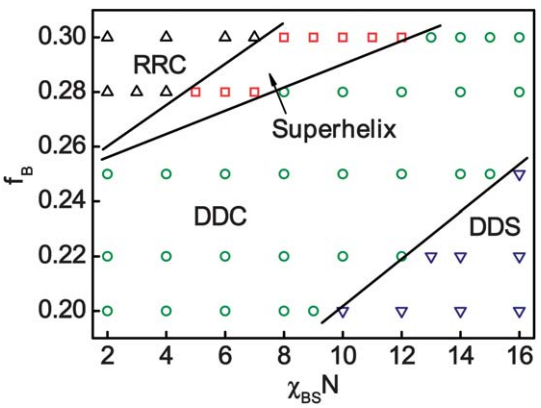

Fig. 5 Observed structure regions as a function of $\chi_{BS}N$ at different values of f_B for ABC terpolymers with equal lengths of A and C end-blocks in a selective solvent. Each point corresponds to a simulation result, and the lines are drawn to identify the boundaries between different structures.

As can be seen from Fig. 5, in addition to the **RRC**, **DDC**, and **DDS** microstructures, a new structural motif—double-stranded superhelix—was identified in the calculations. Fig. 6 provides detailed information on the double-stranded helical superstructure. In the double-stranded superhelix, the A and C blocks form each helix, while the B midblocks knit them together and simultaneously form the shell to wrap around the solvophobic cores. Taking the ABC terpolymer solutions with $f_A = f_C = 0.35$ and $\chi_{BS}N = 10.0$ as an example, the superhelix has diameters of approximately $4.7R_g$ and a pitch of approximately $4.0R_g$. The double-stranded superhelix is an interesting finding of the present work, and understanding the appearance of the superhelix in the **RRC** → superhelix → **DDC** transition could be of significance for designing biological materials and advanced functional materials.

We further analyzed the free energy variations upon the formation of the superhelix. Fig. 7 shows the changes of free energy, interaction enthalpy, and configurational entropy of the terpolymer aggregates upon increasing the $\chi_{BS}N$ value. As can be seen from Fig. 7a, the superhelix is shown to be more stable than the structures of **DDC** and **RRC** at the intermediate $\chi_{BS}N$ value. The reason that the superhelix is more stable at the intermediate $\chi_{BS}N$ value arises from the interplay of enthalpic and entropic effects. When the superhelix is being formed during $\chi_{BS}N$ increases, the loss of configurational entropy becomes less than that of **RRC** (Fig. 7b). This is because the solvophobic cores reorganize themselves from ring-like cylinders to helix-like cylinders in the **RRC** → superhelix transition, resulting in the relaxation of chain stretching. However, such a rearrangement of

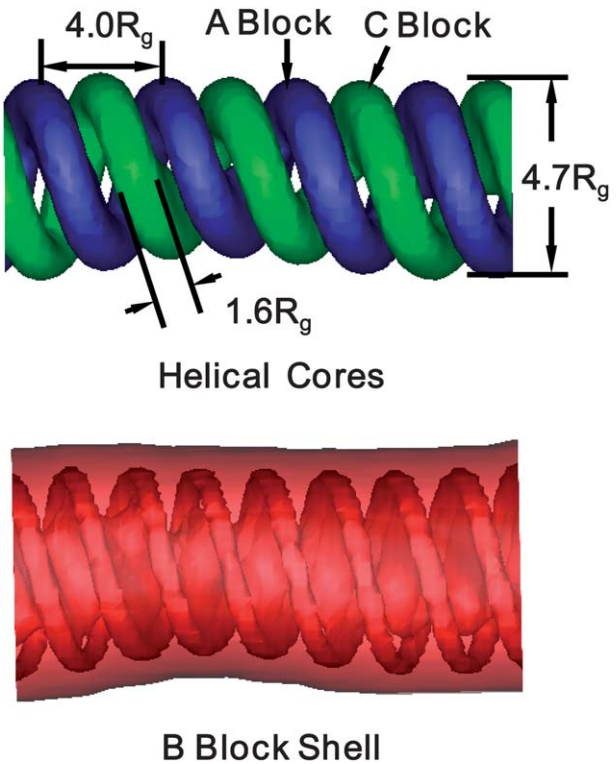

Fig. 6 A superhelix self-assembled from ABC terpolymers in a selective solvent with $f_A = f_C = 0.35$ and $\chi_{BS}N = 10.0$. For clarity, the solvophobic cores and solvophilic shell are presented separately. The colors appear as in Fig. 2.

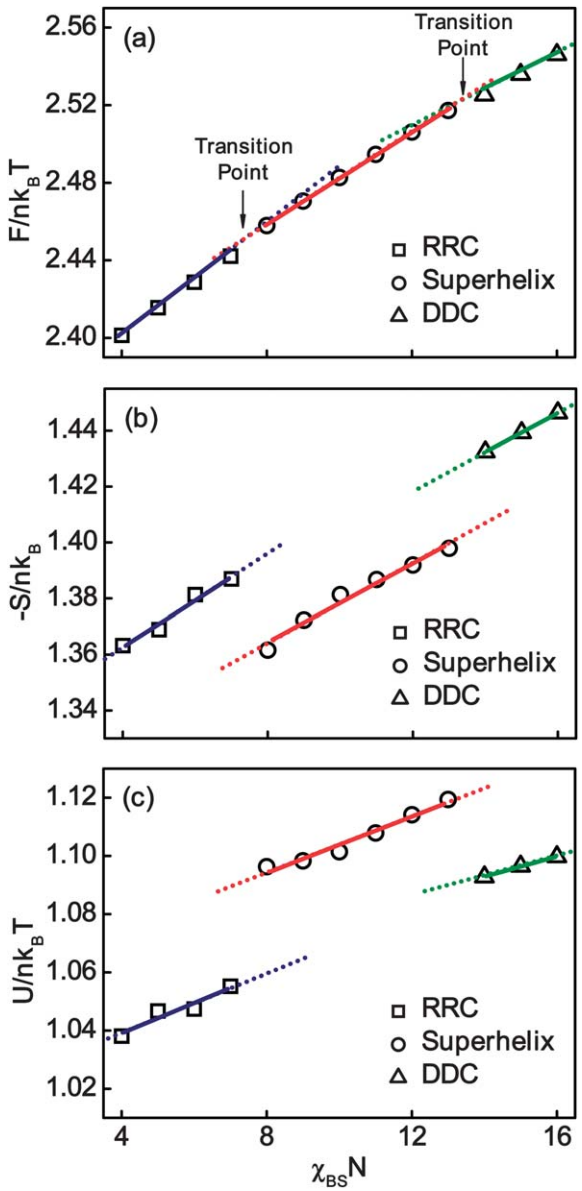

Fig. 7 Plots of (a) free energy F, (b) configurational entropy S, and (c) internal energy U as a function of $\chi_{BS}N$ for various microstructures. The relative lengths of the solvophobic blocks is $f_A = f_C = 0.35$.

cores results in unfavorable interaction enthalpies (Fig. 7c). At the point where the entropic effect overwhelms the enthalpic effect, the superhelix appears. When $\chi_{BS}N$ continuously increases, the superhelix cannot be maintained due to the dramatic increase in enthalpy. To compensate the effect of the increase in enthalpy, a **DDC** structure is formed. In the superhelix → **DDC** transition, the solvophobic cores change from cylinders to disks, giving rise to the reduction of relative surface areas. This change in interfacial curvatures leads to an optimization of enthalpy ($U/n\mathrm{k_B}T$ decreases as the superhelix →**DDC** transition occurs) but an increase in configurational entropy losses. The breakdown of the superhelix is a consequence of the combined enthalpic and entropic effects.

The multicore micelle, presenting more hierarchy than the widely-observed aggregates such as spherical micelles and vesicles, is an interesting phenomenon. In this work, we predicted a previously unknown class of multicore micelles in which multiple solvophobic cores are associated with solvophilic blocks into a hierarchical order. It has been well-known that the linear *ABC* terpolymers are capable of forming mixed corona micelles, core–shell–corona micelles, and core–inner corona–outer corona micelles, depending on the solvent's selectivity towards each block.[58] However, less attention has been paid to the present case that the solvent is only selective for the middle blocks, because it was commonly recognized that self-organization of such a system could only result in "two populations of micelles" rather than coherent compartmentalized micelles,[6,59] *i.e.*, multi-compartment micelles or multicore micelles. The difference between the "two populations of micelles" and multicore micelles is that the solvophobic cores in the "two populations of micelles" are disordered, while the solvophobic cores in the multicore micelle are regularly organized. In these two cases, the enthalpy is almost identical, but the entropy is different. The interplay of the configurational entropy of midblock and translational entropy of cores determine the final state. Compared with the multicore micelles, in the "two populations of micelles", a disordered arrangement of cores increases the translational entropy of cores, but decreases the configurational entropy of the midblock due to the unfavorable confinement from the cores. The configurational entropic loss of the midblock is dependent on the length of the midblock. When the midblock is relatively longer, the confinement imposed by solvophobic cores is reduced, and thus the effect of the packing of solvophobic cores on the configurational entropic loss of the midblock becomes less pronounced. In this sense, the transitional entropy dominates the micelle formations, and the "two populations of micelles" is preferred. Therefore, the multicore micelles are formed at short midblocks, while the "two populations of micelles" is favored at longer midblocks.

In addition to our results, recent experiments also provided evidence that the linear *ABC* terpolymers with solvophilic midblocks are able to self-assemble into compartmentalized micelles.[25,26] Laschewsky *et al.* provided a visualization of the compartmentalized raspberry-like micelles self-assembled from the (FDA)–(OEGA)–(EHA) terpolymers with fluorophilic–hydrophilic–lipophilic block sequence, where FDA, OEGA, and EHA are 1*H*,1*H*,2*H*,2*H*-perfluorodecyl acrylate, oligoethyleneglycolmonomethylether acrylate, and 2-ethylhexyl acrylate, respectively.[25,26] The cryogenic transmission electron microscopy observation revealed that the formed raspberry-like micelles have a hierarchical structure. The fluorophilic block forms irregular patches near the core/corona interface and the tube-walls within the central core region, while the lipophilic block forms the spherical matrix. These raspberry-like micelles with characteristics of multicore micelles are identical to the **SV** (Fig. 3), where fluorophilic, hydrophilic, and lipophilic blocks corresponds to the *A*, *B*, and *C* blocks, respectively.

The SCF calculations can not only reproduce the structure of the raspberry-like micelles observed in experiments, but also provide an insight into the formation mechanism of the raspberry-like micelles (**SV**). In Laschewsky's experiments, an interesting phenomenon observed is that the fluorophilic domains are preferentially located both at the core/corona interface and within the central core region. The SCF calculation is ready to reveal the mechanism behind the formation of such hierarchical

multicore structures. In Laschewsky's experiments, the most studied molecule is $(FDA)_{40}$–$(OEGA)_{50}$–$(EHA)_{120}$ terpolymers. For a comparison, the volume fraction of *A*, *B*, and *C* blocks was set to be 25%, 20%, and 55%, corresponding to that of FDA, OEGA, and EHA blocks, respectively. In addition, the Flory–Huggins parameters $\chi_{AB}N$, $\chi_{BC}N$, $\chi_{BS}N$, and $\chi_{CS}N$ were set as used in Fig. 3. Such chosen parameters are not intended to represent a specific chemistry of the $(FDA)_{40}$–$OEGA)_{50}$–$(EHA)_{120}$ terpolymer but are intended to capture the characteristics of the raspberry-like micelle formation. Fig. 8 shows the results obtained at various $\chi_{AC}N$ and $\chi_{AS}N$ values. When $\chi_{AC}N = 20.0$ and $\chi_{AS}N = 50.0$, the *ABC* terpolymers self-assembled into the micelles with patches residing near the core/corona interface and tubes embedding into the central core, as shown in Fig. 8a. This micelle is the so-called raspberry-like micelle (**SV**) as observed in the experiments. When $\chi_{AS}N$ decreases to 30.0 and $\chi_{AC}N$ remains as 20.0, a different micelle was formed, as shown in Fig. 8b. In this micelle, a fraction of *A* blocks forms tubes within the central core, while the remainder covers the outer surface of *C* core homogeneously. As $\chi_{AC}N$ decreases to 5.0 and $\chi_{AS}N$ fixes as 30.0, a conventional vesicle was observed (Fig. 8c). In this vesicle, both the inner and outer surfaces of *C* core was homogeneously covered with *A* blocks.

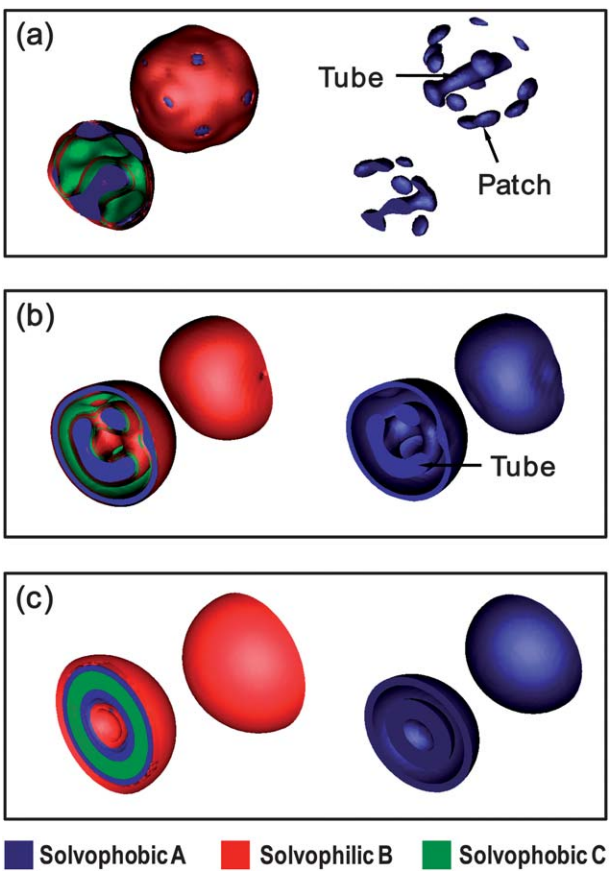

Fig. 8 Multicore micelles self-assembled from *ABC* terpolymers with $f_A = 0.25$, $f_B = 0.20$, $f_C = 0.55$, $\chi_{AB}N = 20.0$, $\chi_{BC}N = 20.0$, $\chi_{BS}N = 2.0$, and $\chi_{CS}N = 40.0$ in a selective solvent. The other parameters are (a) $\chi_{AC}N = 20.0$ and $\chi_{AS}N = 50.0$; (b) $\chi_{AC}N = 20.0$ and $\chi_{AS}N = 30.0$; (c) $\chi_{AC}N = 5.0$ and $\chi_{AS}N = 30.0$. The left shows the whole structures, while the right shows the structure formed by *A* blocks. The colors appear as in Fig. 2.

Comparing Fig. 8a with Fig. 8b, we learn that a lower selectivity of solvent for *A* blocks (relative to *C* blocks) is helpful for forming patches at the core/corona interface. Because the *A* blocks are linked to solvophilic *B* midblocks, the *A* domains must locate at the core/corona interface. As the solvents become more incompatible to *A* blocks than to *C* blocks, the *A* blocks are aggregated to minimize the contact with solvents, thereby producing the patches at the core/corona interface. Moreover, comparison of Fig. 8b and Fig. 8c indicates that the formation of tubes within the central core region originates from the unfavorable interaction between *A* and *C* blocks. The formation of tubes in the core region can efficiently separate *A* blocks from *C* blocks and thus reduce the interaction enthalpy between *A* and *C* blocks. From the above perspective, we conclude that optimizing the interaction energy between *A* (FDA) blocks and the solvents drives the formation of patches near the core/corona interface, whereas minimizing the contact between *A* (FDA) and *C* (EHA) blocks induces the formation of tubes within the central core. This conclusion supports the speculations proposed by Laschewsky *et al.* well. They suggested that the formation of fluorophilic patches at the surface of the lipophilic core is due to the connection between the fluorophilic block and the corona-forming hydrophilic block, while the formation of fluorophilic tubes within the lipophilic core is ascribed to the formation of inverse micelle-like aggregates as in the large-compound micelle.

In addition to the pure *ABC* terpolymer solutions, we also found some evidence of multicore micelles which were prepared from mixture systems containing terpolymers and multiamine counterions. Pochan *et al.*, for example, prepared a cylinder with alternating stripes perpendicular to the cylinder axes, which is very similar to the **DDC** structure, *via* kinetic control of block copolymer assemblies.[22] The technology relies on the divalent organic counter ions to drive the organization of block copolymers micelles into a complex structure. Furthermore, they created a double helical superstructure through uniformly coiling cylindrical micelles with multiamines.[23] In contrast to Pochan's design, we demonstrate herein a one-step solution assembly strategy for multicore micelles from the *HPH* linear *ABC* terpolymer solutions. Our theoretical predictions offer a simple, feasible, and promising method for preparing multicore micelles.

At the end of the work, we wish to emphasize that, although the present calculations can capture the essential feature of experimental observations, there are several drawbacks in the calculations. First, the Helmholtz free energy was used to represent an entire macroscopic system, which is not realistic for a dilute solution. Second, a higher concentration was adopted in the calculations. For such a chosen concentration, some simulation points may be located at the region close to the spinodal line, which allows the micelles to be easily formed by quenching from an initial homogeneous solution. A rational method is to use excess grand potential, which is not only a function of the temperature (χ), but also a function of the chemical potential (concentration).[49,60,61] Very recently, Wang *et al.* studied the micelles formed by a coil–comb block copolymer by calculating the excess free energy of formation of a micelle in a dilute solution.[62] The results demonstrated that the micelle structures are greatly dependent on the concentration of single chains, which is

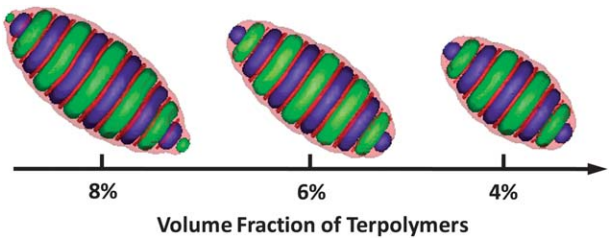

Fig. 9 Multicore micelle structures as a function of the volume fraction of terpolymers for linear *ABC* terpolymers in a selective solvent with $f_A = f_C = 0.40$ and $\chi_{BS}N = 2.0$. The colors appear as in Fig. 2.

consistent with the experimental observations. While Wang's method is powerful and more accurate for dilute solutions, the method is shown to have a limitation, *i.e.*, a preassumption of symmetry is required. Therefore, this method would suffer from the difficulty in predicting unknown morphologies. Compared with Wang's method, the present calculations would miss an important issue, namely, the effect of concentration on micelles. To evaluate such an effect, we calculated the micelles at various concentrations. The result was shown in Fig. 9. When the concentration decreases, the **DDC** micelle is gradually shrunk and transformed into the spindle-like **DDS** micelle, where the number of disk-like cores decreases. This implies that the association number of the multicore micelles decreases as the concentration decreases, which is consistent with the observations in diblock copolymer and coil–comb block copolymer solutions.[62] The concentration is shown to play an important role in determining the structure of multicore micelles. In the future, we will try to use the method proposed by Wang *et al.* to study the competition of length scales in the multicore micelles. More interesting phenomena may be discovered.

IV. Conclusion

Using self-consistent field calculations, we discovered that the linear *ABC* terpolymers with solvophobic–solvophilic–solvophobic block sequences are capable of self-assembling into multicore micelles, such as the double-stranded superhelix, in midblock-selective solvents. The microstructures of multicore micelles can be tuned by changing the relative length of the blocks and the solubility of the midblock, and the corresponding morphological regions were mapped out. These hierarchically ordered multicore micelles were exhibited to possess two different-length-scale structures. The solvophilic midblock plays an important role in connecting the mutually incompatible solvophobic micellar cores into a large-length-scale microstructure, much like the organization of the cells into tissues in biology. The formation of multicore micelles offered a higher level of self-assembly, exceeding that of micelle-like aggregates with single solvophobic cores surrounded by solvophilic shells. The results gained through SCF calculations enrich our existing knowledge of block copolymer self-assembly.

Acknowledgements

This work was supported by National Natural Science Foundation of China (50925308). Supports from projects of Shanghai municipality (09XD1401400, 0952nm05100, 08DZ2230500, and B502) are also appreciated.

References

1 R. F. Service, *Science*, 2005, **309**, 95.
2 C. K. Ober, S. Z. D. Cheng, P. T. Hammond, M. Muthukumar, E. Reichmanis, K. L. Wooley and T. P. Lodge, *Macromolecules*, 2009, **42**, 465–471.
3 I. W. Hamley, *Angew. Chem., Int. Ed.*, 2003, **42**, 1692–1712.
4 M. Muthukumar, C. K. Ober and E. L. Thomas, *Science*, 1997, **277**, 1225–1232.
5 X. Wang, G. Guerin, H. Wang, Y. Wang, I. Manners and M. A. Winnik, *Science*, 2007, **317**, 644–647.
6 A. Laschewsky, *Curr. Opin. Colloid Interface Sci.*, 2003, **8**, 274–281.
7 I. W. Hamley, in *Block Copolymers in Solution: Fundamentals and Applications*, John Wiley & Sons, Hoboken, NJ, 2005.
8 L. Zhang and A. Eisenberg, *Science*, 1995, **268**, 1728–1731.
9 D. E. Disher and A. Eisenberg, *Science*, 2002, **297**, 967–973.
10 W. Kong, B. Li, Q. Jin, D. Ding and A.-C. Shi, *J. Am. Chem. Soc.*, 2009, **131**, 8503–8512.
11 N. Saito, C. Liu, T. P. Lodge and M. A. Hillmyer, *Macromolecules*, 2008, **41**, 8815–8822.
12 Z. Li, E. Kesselman, Y. Talmon, M. A. Hillmyer and T. P. Lodge, *Science*, 2004, **306**, 98–101.
13 N. Saito, C. Liu, T. P. Lodge and M. A. Hillmyer, *ACS Nano*, 2010, **4**, 1907–1912.
14 Z. Li, M. A. Hillmyer and T. P. Lodge, *Langmuir*, 2006, **22**, 9409–9417.
15 A. Walther and A. H. E. Müller, *Chem. Commun.*, 2009, 1127–1129.
16 S. Kubowicz, J.-F. Baussard, J.-F. Lutz, A. F. Thünemann, H. v. Berlepsch and A. Laschewsky, *Angew. Chem., Int. Ed.*, 2005, **44**, 5262–5265.
17 K. Skrabania, A. Laschewsky, H. v. Berlepsch and C. Böttcher, *Langmuir*, 2009, **25**, 7594–7601.
18 R. Wang, P. Tang, F. Qiu and Y. Yang, *J. Phys. Chem. B*, 2005, **109**, 17120–17127.
19 A. F. Thünemann, S. Kubowicz, H. v. Berlepsch and H. Möhwald, *Langmuir*, 2006, **22**, 2506–2510.
20 J. Dupont, G. Liu, K. Niihara, R. Kimoto and H. Jinnai, *Angew. Chem., Int. Ed.*, 2009, **48**, 6144–6147.
21 J. Hu, G. Njikang and G. Liu, *Macromolecules*, 2008, **41**, 7993–7999.
22 H. Cui, Z. Chen, S. Zhong, K. L. Wooley and D. J. Pochan, *Science*, 2007, **317**, 647–650.
23 S. Zhong, H. Cui, Z. Chen, K. L. Wooley and D. J. Pochan, *Soft Matter*, 2008, **4**, 90–93.
24 R. Weberskirch, J. Preudchen, H. W. Spiess and O. Nuyken, *Macromol. Chem. Phys.*, 2000, **201**, 995–1007.
25 H. v. Berlepsch, C. Böttcher, K. Skrabania and A. Laschewsky, *Chem. Commun.*, 2009, 2290–2292.
26 K. Skrabania, H. v. Berlepsch, C. Böttcher and A. Laschewsky, *Macromolecules*, 2010, **43**, 271–281.
27 S.-H. Chou, H.-K. Tsao and Y.-J. Sheng, *J. Chem. Phys.*, 2006, **125**, 194903.
28 S. Kubowicz, A. F. Thünemann, R. Weberskirch and H. Möhwald, *Langmuir*, 2005, **21**, 7214–7219.
29 J.-F. Lutz and A. Laschewsky, *Macromol. Chem. Phys.*, 2005, **206**, 813–817.
30 M. W. Matsen, *J. Phys.: Condens. Matter*, 2002, **14**, R21.
31 G. H. Fredrickson, in *The Equilibrium Theory of Inhomogeneous Polymers*, Oxford University Press, Oxford, 2006.
32 E. M. Lennon, K. Katsov and G. H. Fredrickson, *Phys. Rev. Lett.*, 2008, **101**, 138302.
33 Y. Bohbot-Raviv and Z.-G. Wang, *Phys. Rev. Lett.*, 2000, **85**, 3428–3431.
34 X. Ye, T. Shi, Z. Lu, C. Zhang, Z. Sun and L. An, *Macromolecules*, 2005, **38**, 8853–8857.
35 W. Li and A.-C. Shi, *Macromolecules*, 2009, **42**, 811–819.
36 D. M. Patel and G. H. Fredrickson, *Phys. Rev. E: Stat. Phys., Plasmas, Fluids, Relat. Interdiscip. Top.*, 2003, **68**, 051802.
37 L. Wang, J. Lin and L. Zhang, *Macromolecules*, 2010, **43**, 1602–1609.
38 L. Zhang, J. Lin and S. Lin, *Soft Matter*, 2009, **5**, 173–181.
39 M. W. Matsen, *Macromolecules*, 1995, **28**, 5765–5773.

40 N. Koneripalli, R. Levicky, F. S. Bates, M. W. Matsen, S. K. Satija, J. Ankner and H. Kaiser, *Macromolecules*, 1998, **31**, 3498–3508.
41 R. B. Thompson, V. V. Ginzburg, M. W. Matsen and A. C. Balazs, *Macromolecules*, 2002, **35**, 1060–1071.
42 R. B. Thompson, V. V. Ginzburg, M. W. Matsen and A. C. Balazs, *Science*, 2001, **292**, 2469–2472.
43 L. Zhang and J. Lin, *Macromolecules*, 2009, **42**, 1410–1414.
44 X. He and F. Schmid, *Phys. Rev. Lett.*, 2008, **100**, 137802.
45 X. He, H. Liang, L. Huang and C. Pan, *J. Phys. Chem. B*, 2004, **108**, 1731–1735.
46 Y. Jiang, T. Chen, F. Ye, H. Liang and A.-C. Shi, *Macromolecules*, 2005, **38**, 6710–6717.
47 L. Zhang, J. Lin and S. Lin, *J. Phys. Chem. B*, 2007, **111**, 9209–9217.
48 L. Zhang, J. Lin and S. Lin, *Macromolecules*, 2007, **40**, 5582–5592.
49 D. Duque, *J. Chem. Phys.*, 2003, **119**, 5701–5704.
50 F. Drolet and G. H. Fredrickson, *Phys. Rev. Lett.*, 1999, **83**, 4317–4320.
51 V. Ganesan and G. H. Fredrickson, *Europhys. Lett.*, 2001, **55**, 814–820.
52 G. H. Fredrickson, V. Ganesan and F. Drolet, *Macromolecules*, 2002, **35**, 16–39.
53 G. Tzeremes, K. Ø. Rasmussen, T. Lookman and A. Saxena, *Phys. Rev. E: Stat. Phys., Plasmas, Fluids, Relat. Interdiscip. Top.*, 2002, **65**, 041806.
54 K. Ø. Rasmussen and G. Kalosakas, *J. Polym. Sci., Part B: Polym. Phys.*, 2002, **40**, 1777–1783.
55 V. Eyert, *J. Comput. Phys.*, 1996, **124**, 271–285.
56 J. U. Kim and M. W. Matsen, *Soft Matter*, 2009, **5**, 2889–2895.
57 J. Ma, X. Li, P. Tang and Y. Yang, *J. Phys. Chem. B*, 2007, **111**, 1552–1558.
58 N. Hadjichristidis, H. Iatrou, M. Pitsikalis, S. Pispas and A. Avgeropoulos, *Prog. Polym. Sci.*, 2005, **30**, 725–782.
59 R. Shunmugam, C. E. Smith and G. N. Tew, *J. Polym. Sci., Part A: Polym. Chem.*, 2007, **45**, 2601–2608.
60 S. M. Wood and Z.-G. Wang, *J. Chem. Phys.*, 2002, **116**, 2289–2300.
61 N. A. M. Besseling and M. A. Cohen Stuart, *J. Chem. Phys.*, 1999, **110**, 5432–5436.
62 J. Wang, K. Guo, L. An, M. Müller and Z.-G. Wang, *Macromolecules*, 2010, **43**, 2037–2041.